



HAL
open science

Synthesis and Characterization of Ruffled Phosphorus meso -Ester Corroles

Di Gao, Cloé Azarias, Anthony d'Aléo, Michel Giorgi, Olivier Siri, Teodor
Silviu Balaban, Denis Jacquemin, Gabriel Canard

► **To cite this version:**

Di Gao, Cloé Azarias, Anthony d'Aléo, Michel Giorgi, Olivier Siri, et al.. Synthesis and Characterization of Ruffled Phosphorus meso -Ester Corroles. *European Journal of Inorganic Chemistry*, 2017, 2017 (4), pp.780 - 788. 10.1002/ejic.201601172 . hal-01683282

HAL Id: hal-01683282

<https://hal.science/hal-01683282>

Submitted on 14 Apr 2018

HAL is a multi-disciplinary open access archive for the deposit and dissemination of scientific research documents, whether they are published or not. The documents may come from teaching and research institutions in France or abroad, or from public or private research centers.

L'archive ouverte pluridisciplinaire **HAL**, est destinée au dépôt et à la diffusion de documents scientifiques de niveau recherche, publiés ou non, émanant des établissements d'enseignement et de recherche français ou étrangers, des laboratoires publics ou privés.

Synthesis and Characterization of Ruffled Phosphorus *meso*-Ester Corroles

Di Gao,^[a] Cloé Azarias,^[b] Anthony D'Aléo,^[c] Michel Giorgi,^[d] Olivier Siri,^[c]
Teodor Silviu Balaban,^[a] Denis Jacquemin,^{*,[b,e]} and Gabriel Canard^{*,[c]}

Abstract: The strong electron-withdrawing character of 5,15-*meso*-ester groups was demonstrated through the study of four fluorescent hexacoordinate phosphorus(V) *meso*-substituted corroles, which were characterized by various techniques including single-crystal X-ray diffraction and first-principles calcu-

lations. The nature of the remaining *meso* substituent tunes the physicochemical properties of these phosphorus complexes only slightly but unexpectedly plays a key role in the ruffling of the macrocycle.

Introduction

During the last fifteen years, the corrole macrocycle has emerged as one of the most studied porphyrin analogues, because several synthetic methods are now available for the gram-scale preparation of such derivatives.^[1] Consequently, corroles and their metal complexes have been used in a large variety of research domains such as catalysis,^[2] sensors,^[3] electronic devices^[4] and medicine.^[5] The future development of corrole-based materials and devices will probably require compounds featuring refined and controlled physicochemical properties.

These properties can be tuned through different strategies. For example, the introduction of multiple bulky peripheral substituents can produce slightly to highly distorted macrocycles and thereby redshift their light absorption maxima.^[6] Nevertheless, these modifications are only efficient in metallic derivatives in which a noninnocent ligand is used.^[7] A more generic approach to modify the electronic and spectroscopic features of corrole derivatives is to tune or extend their π system. This strategy was effective in derivatives in which the conjugation of the corrole ring was extended through its fusion with aromatic rings such as benzenes, quinones, pyrazines or even a

second corrole moiety.^[8] The corrole properties can also be modulated by more straightforward peripheral modifications such as the introduction of one or more conjugated functional groups including formyl, nitro, carboxy or chlorosulfonyl groups.^[9]

We have recently explored this topic through the synthesis and characterization of multiple corrole free bases bearing *meso*-ester groups.^[10] These particular substituents stabilize corrole free bases against oxidation and induce redshifts of their light absorption and emission bands. We chose phosphorus as the first chelated element since P^V-corroles are highly fluorescent derivatives,^[11] which have been employed widely as photosensitizers,^[12] imaging probes in biological applications^[13] and in the construction of photoactive arrays.^[14] We report herein the preparation and characterization of four new phosphorus(V) 5,15-diester corroles, which were studied by several techniques including cyclic voltammetry, single-crystal X-ray diffraction and time-dependent density functional theory (TD-DFT) calculations, which show how the electron-withdrawing character of the *meso*-ester groups is increased by their π overlap with the macrocyclic aromatic system. This work also demonstrates that the physicochemical properties of such derivatives are only tuned slightly by the nature of the third *meso* substituent, which has, in contrast, a strong influence on the out-of-plane distortion of the macrocycle.

Results and Discussion

Synthesis

Several groups have studied the physicochemical properties and reactivities of *meso*-substituted phosphorus(V) corrole complexes, which can be prepared through the addition of PCl₃ or POCl₃ to solutions of corrole free bases in pyridine.^[11a,15] We selected the latter conditions to prepare four new phosphorus(V) 5,15-*meso*-ester corroles **1-P**, **2-P**, **3-P** and **4-P**, in which the remaining *meso* position is occupied by a third ester

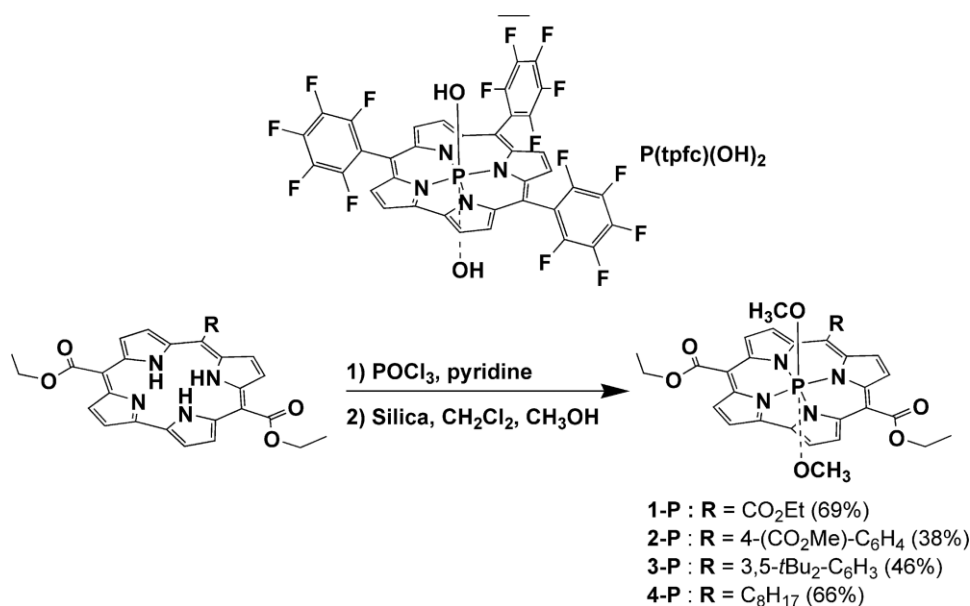
[a] Aix Marseille Univ, CNRS, Centrale Marseille, ISM2, Chirosciences, 13288 Marseille Cedex 09, France

[b] Laboratoire CEISAM, Université de Nantes, CNRS, 2 rue de la Houssinière, 44322 Nantes Cedex 03, France
E-mail: Denis.Jacquemin@univ-nantes.fr
<http://www.sciences.univ-nantes.fr/CEISAM/>

[c] Aix Marseille Univ, CNRS, CINaM, Campus de Luminy, Case 913, 13288 Marseille Cedex 09, France
E-mail: gabriel.canard@univ-amu.fr
<http://www.cinam.univ-mrs.fr/cinam/>

[d] Aix Marseille Univ, Spectropole, 13288 Marseille Cedex 09, France

[e] Institut Universitaire de France (IUF) 1 rue Descartes, 75005 Paris Cedex 05, France



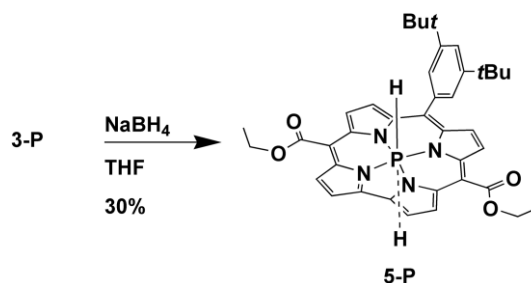
Scheme 1. Structure of the previously reported compound P(tpfc)(OH)₂ and the synthesis of the phosphorus(V) 5,15-*meso*-ester corroles **1-P**, **2-P**, **3-P** and **4-P**.

group (**1-P**), a long alkyl chain (**4-P**) or an aryl group displaying either electron-withdrawing (**2-P**) or electron-donating character (**3-P**, Scheme 1). The physicochemical properties of these complexes were compared to those reported for the hexacoordinate phosphorus(V) compound P(tpfc)(OH)₂ [tpfc = 5,10,15-tris(pentafluorophenyl)corrole], in which the macrocycle has three strongly electron-withdrawing pentafluorophenyl substituents.^[16]

The addition of POCl₃ to *meso*-triarylcorroles in pyridine under reflux produces P^V complexes in which the central ion is coordinated by one or two axial hydroxy ligands.^[15,16] In our hands, the synthesis produced only the hexacoordinate complexes **1-P**, **2-P**, **3-P** and **4-P** bearing two axial methoxy ligands owing to the use of methanol during the chromatographic purification with silica gel (Scheme 1). For each compound, the ¹H NMR spectrum contained only four signals for the β-hydrogen atoms (see the Supporting Information) and confirmed a single coordination mode, whereas the single signal located close to δ = -184 ppm observed in the four ³¹P NMR spectra was the signature of these hexacoordinate species.^[15b] Nevertheless, these hexacoordinate complexes are prone to ligand dissociation if their substituents are electron-donating or if they are dissolved in non-coordinating solvents.^[15b] Although use of bulky electron-donating siloxy groups^[15d] or fluoride ligands^[15c] limits this dissociation, our study is focused on the properties of the hexacoordinate complexes **1-P**, **2-P**, **3-P** and **4-P** because (1) they are stabilized by strongly electron-withdrawing *meso*-ester groups (see below) and (2) they were studied in a coordinating solvent (CD₃OD) or in freshly prepared solutions containing a few drops of methanol.

The expected reduction of the ester groups of **3-P** with an excess of NaBH₄ produced the dihydrido phosphorus(V) complex **5-P** together with a complex mixture of coloured species lacking aromaticity, as no Soret bands featured in their UV/Vis spectra (Scheme 2). This axial substitution of the central P^V ion

is already known.^[15c,17] Nevertheless, as for the corresponding free-base series, the concomitant and major loss of the corrole material shows that the transformation of electron-withdrawing 5,15-*meso* substituents into strongly electron-donating ones probably produces unstable compounds that rapidly decompose into stable isocorrole species^[18] or open-chain macrocycles.^[19]



Scheme 2. Synthesis of the dihydrido phosphorus(V) 5,15-*meso*-ester corrole **5-P**.

Crystal Structures of **1-P**, **2-P**, **3-P** and **4-P**

The slow diffusion of *n*-heptane into concentrated dichloromethane solutions of **1-P**, **2-P** and **4-P** containing a few drops of methanol yielded single crystals suitable for X-ray analysis, which was also conducted with a crystal of **3-P** grown serendipitously from a solution of this compound in CD₃OD (Figures 1 and S1 in the Supporting Information). Details of the experimental structure determinations are given in the Experimental Section, and the structural data can be found in Table S1. The structures of **2-P**, **3-P** and **4-P** suffer from partial disorder of the alkyl moieties or the *meso*-ester groups, but we are confident that the corresponding structural solutions and data refinements are of high enough quality to allow us to com-

ment on the environments of the central P^V ions and the distortions affecting the macrocycle.

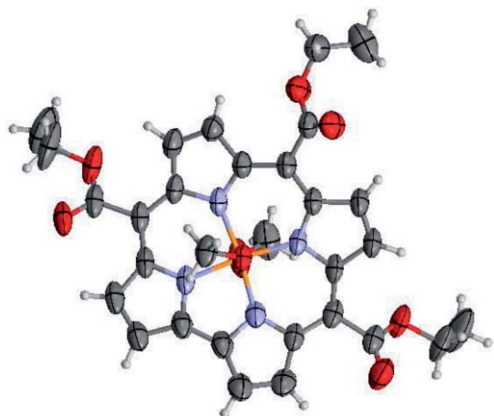


Figure 1. ORTEP view of corrole **1-P** (the structures of **2-P**, **3-P** and **4-P** are reported in the Supporting Information).

In the four structures, the P atoms are coordinated octahedrally and lie in the mean plane of the four nitrogen atoms (denoted \bar{N}), as illustrated by the corresponding out-of-plane displacements that are smaller than 0.02 Å. The P coordination is completed by the oxygen atoms of two methoxide groups with P...O distances of ca. 1.66 Å, which are similar to those reported for analogous hexacoordinate phosphorus(V) corroles displaying axial alkoxido or hydroxido ligands.^[15b,15d,20] The most interesting feature of the four structures is the ruffling of the corrole macrocycle, the amplitude of which increases with the electron-withdrawing character of the 10-*meso* substituent (Figure 2). This distortion was recently evidenced for the first time in the structures of phosphorus(V) *meso*-triarylcorroles bearing up to seven β -bromine atoms and can be described by the ruffling angle Ψ (defined as the torsion angle between the C6-N22 and C16-N24 bonds in Figure 2) or the distances between the mean plane \bar{N} and the *meso* carbon atoms C5 (C5... \bar{N}), C10 (C10... \bar{N}) and C15 (C15... \bar{N} , Figure 2 and Table 1).^[20] The ruffling of the macrocycle puts the C5 and C15 atoms above the \bar{N} plane and the C10 atom on the opposite side (Figure 2).

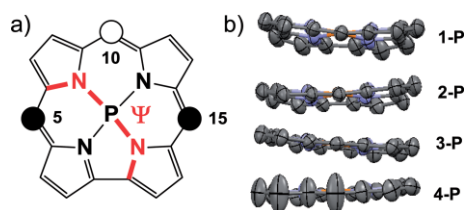


Figure 2. (a) Schematic representation of the ruffling torsion angle Ψ (the filled circles correspond to the *meso* carbon atoms C5 and C15 that are above the \bar{N} mean plane, and the open circle represents the carbon atom C10 that lies below this plane); (b) views of the ruffled macrocycles of P^V corroles **1-P**, **2-P**, **3-P** and **4-P** along the C10-P axis (the peripheral substituents and axial methoxy groups are omitted for clarity).

As in β -bromo-*meso*-triaryl derivatives, the largest distances to the \bar{N} plane are those involving the central *meso* carbon atom (C10), which reach 0.53 Å (Table 1). This position also has an important impact on the out-of-plane distortion of the

Table 1. Geometric parameters of **1-P**, **2-P**, **3-P** and **4-P**.

	C5... \bar{N} [Å]	C10... \bar{N} [Å]	C15... \bar{N} [Å]	Ψ [°]
1-P	0.37	0.53	0.28	16
2-P	0.30	0.39	0.18	12
3-P	0.21	0.14	0.13	8
4-P	0.23	0.14	0.06	10

macrocycle, which increases with the electron-withdrawing character of the 10-*meso* substituent. For example, if the 3,5-di-*tert*-butylphenyl group of **3-P** is replaced by an aryl group bearing an ester moiety in **2-P**, the C10... \bar{N} distance increases from 0.14 to 0.39 Å, whereas the ruffling angle Ψ increases by 50 %. These trends cannot be explained yet but are in accordance with those reported previously.^[20]

Electrochemical Analysis

The cyclic voltammograms of **1-P**, **2-P**, **3-P** and **4-P** dissolved in dichloromethane containing 0.1 M $[nBu_4N][PF_6]$ were recorded. Two typical voltammograms recorded for corrole **2-P** are shown in Figure 3, and all of the half-wave potentials ($E_{1/2}$) are reported in Table 2. The data will be compared with those of the 5,10,15-trispentafluorophenyl derivative $P(tpfc)(OH)_2$ measured under similar experimental conditions.^[16] For each new compound, two irreversible reduction processes and up to three oxidation waves were detected (Figure 3). The first oxidation process is the only reversible one and probably produces a stable hexacoordinate P^V radical cation, as was reported recently.^[16] In contrast, two oxidation waves are observed for the reverse scan in the positive direction just after the first reduction process, probably producing a radical anion involved in a partial axial ligand dissociation.

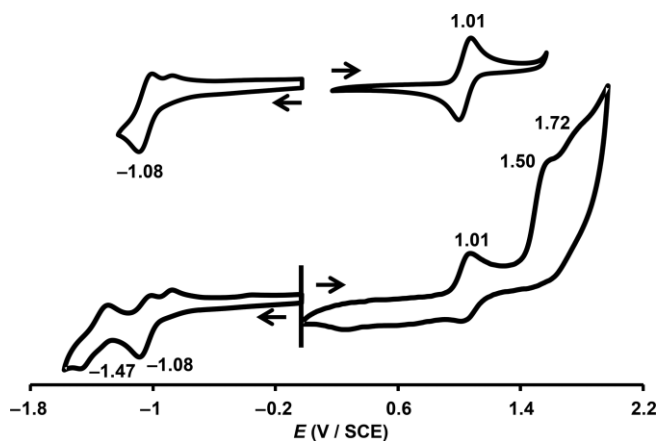


Figure 3. Cyclic voltammograms of corrole **2-P** in CH_2Cl_2 containing 0.1 M $[nBu_4N][PF_6]$ (scan rate 100 mV/s).

Anodic shifts of all of the redox processes are observed if the *meso*-aryl groups of $P(tpfc)(OH)_2$ are replaced by ester groups in **1-P** (Table 2). These small positive shifts illustrate the significant electron-withdrawing character of the ester substituents, which are even slightly more electron-withdrawing than the pentafluorophenyl groups. As in the free-base series, the nature of the 10-*meso* substituent has a low impact on the electrochemi-

Table 2. UV/Vis absorption data,^[a] fluorescence data^[a] and half-wave potentials^[b] [V vs. SCE] of corroles P(tpfc)(OH)₂, **1-P**, **2-P**, **3-P** and **4-P**.

Compound	Absorption data			Electrochemical data			Fluorescence data		
	Soret band [nm] ^[c]	Q bands [nm]	Reduction [V]	Oxidation [V]	ΔE [V]	λ_{em} [nm] ^[d]	$[\Phi]$ ^[e]	τ [ns]	
P(tpfc)(OH) ₂ ^[f]	410	560, 582	-1.05 ^[g]	1.05 ^[g]	2.10	–	–	–	
1-P	418	507, 545, 585	-1.42, -1.03	1.11, 1.76, 1.83	2.14	607, 650	0.12	1.99	
2-P	418	509, 548, 592	-1.47, -1.08	1.01, 1.50, 1.72	2.09	605, 658	0.23	2.66	
3-P	418	510, 550, 594	-1.46, -1.07	0.97, 1.47, 1.71	2.04	607, 660	0.20	2.61	
4-P	418	511, 552, 598	-1.47, -1.07	0.95, 1.46, 1.65	2.02	609, 663	0.28	2.42	

[a] Recorded in aerated CH₂Cl₂ at 298 K. [b] Measured in CH₂Cl₂ containing 0.1M [nBu₄N][PF₆] (scan rate 100 mV/s). [c] The presence of a shoulder of the Soret band is detected for all compounds and is reported in the Experimental Section. [d] λ_{max} for the two bands derived from the corrected emission spectra. [e] Luminescence quantum yields in air-equilibrated dichloromethane, determined by comparison of the corrected emission spectra with that of tetraphenylporphyrin (TPP) in aerated toluene as a standard ($\Phi_{fl} = 0.11$),^[21] excitation at $\lambda = 575$ nm. [f] From ref.^[16] [g] From ref.^[16] recorded in CH₂Cl₂ containing 0.1M [nBu₄N][ClO₄].

cal properties of phosphorus(V) corroles. For example, the first oxidation process located at 1.11 V versus the saturated calomel electrode (SCE) for the 10-ester derivative **1-P** is shifted by less than 70 mV along the **1-P** to **4-P** series. The same slight variation affects the first reduction process, which has a potential ranging from -1.03 to -1.08 V versus SCE. Nevertheless, the $E_{1/2}$ values still increase with the electron-withdrawing character of the 10-*meso* substituent (Table 2).

Photophysical Properties

The absorption and corrected emission spectra of corroles **1-P**, **2-P**, **3-P** and **4-P** in dichloromethane are shown in Figures 4 and S2. The absorption maxima of all of the compounds are collected in Table 2 together with the corresponding emission maxima (excitation at $\lambda = 570$ nm), fluorescence quantum yields and lifetimes. All of the compounds exhibit a typical and intense Soret-type band at $\lambda = 418$ nm and three Q bands in the $\lambda = 500$ –600 nm region (Figure 4).

If the pentafluorophenyl groups of P(tpfc)(OH)₂ are replaced with ester groups in **1-P**, the absorption bands are redshifted by 3 to 15 nm (Table 2). On the other hand, the absorption spectra of **3-P** and **4-P** are almost identical although they bear an aryl group and an alkyl chain at their respective 10-*meso* positions. These results again indicate the higher impact of the 5,15-*meso*-ester groups, which are tightly coupled with the aromatic macrocycle. Nevertheless, the increasing electron-donating properties of the group appended to the 10-position along the **1-P** to **4-P** series still produce slight supplementary redshifts to all of the absorption bands. Similar limited impacts of the electron-donating or -withdrawing *meso* groups on the positions of the absorption bands were observed for the phosphorus(V) *meso*-triarylcorrole series.^[15b,15d]

The four phosphorus(V) 5,15-diester derivatives exhibit relatively intense and structured emission with fluorescence lifetimes in the nanosecond time scale (Table 2). Excitations in the Soret-band region ($\lambda = 370$ –430 nm) or in the Q bands ($\lambda = 500$ –600 nm) produced the same luminescence properties. Small redshifts of the emission spectra are observed if the electron-donating substituents are placed at the 10-position. This trend parallels that observed in the absorption spectra. If corrole **1-P** is set apart, all of the other corrole derivatives have similar quantum yields close to 0.25 and fluorescence lifetime

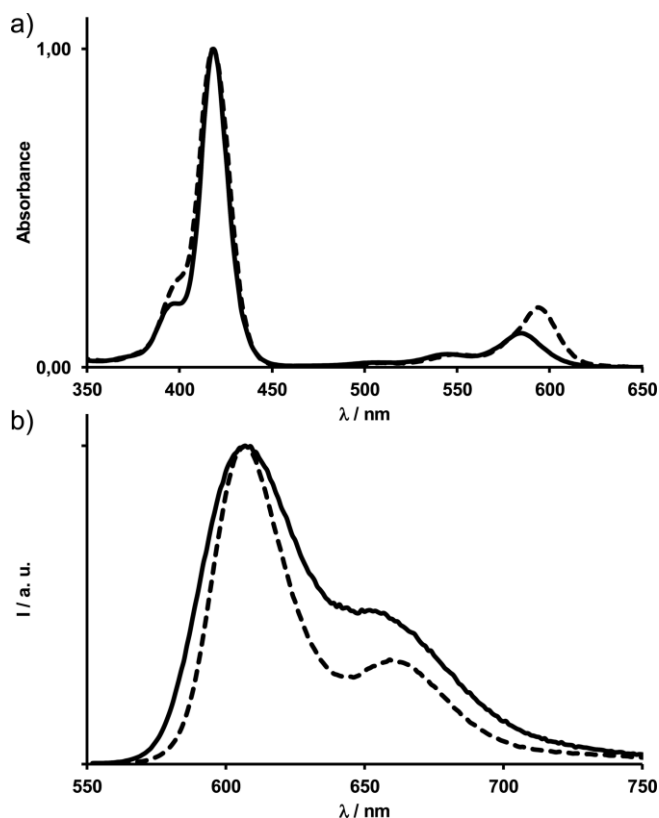


Figure 4. (a) Normalized absorption spectra and (b) normalized corrected emission spectra (excitation at $\lambda = 570$ nm) of phosphorus corroles **1-P** (solid line) and **3-P** (dashed line) in aerated dichloromethane solutions at room temperature.

in the range 2–3 ns, which are similar to those reported for analogous hexacoordinate phosphorus(V) corroles.^[15b,15d,16] The dissolution of **1-P** bearing a third *meso*-ester group in a less polar solvent (toluene) did not increase its fluorescence quantum yield. This partial fluorescence quenching could be due to an electron-transfer process involving the third ester group such as in tryptophan derivatives.^[22]

Theoretical Studies

The effects of the 5,15-*meso*-ester groups on the structural, electronic and optical properties of P^V corroles were investi-

gated theoretically by DFT and TD-DFT methods. The geometry optimizations were performed without symmetry constraints in the gas phase and in dichloromethane with the single-crystal X-ray structures of corroles **1-P**, **2-P**, **3-P** and **4-P** as starting points.

The Kohn–Sham molecular orbital (MO) energies of the two highest occupied (HOMOs) and the two lowest unoccupied molecular orbitals (LUMOs) involved in the Gouterman model are listed in Table 3, their topologies are displayed in Figures 5 and S3, and the electronic transitions involved in the Q and Soret bands for each molecule are listed in Tables 4 and S2. The experimental electrochemical gaps (Table 2) are better correlated if the optical gap (OG) is considered, although correct trends are also provided using the fundamental gap (difference between the ionization potential and electron affinity, Table 3).^[23] The convoluted UV/Vis spectra shown in Figure S4 are in good agreement with the experimental ones, especially the separation between the Soret and Q bands (error ≤ 0.2 eV, typical with TD-DFT).^[24]

Table 3. Calculated Kohn–Sham orbital energies [eV] and theoretical HOMO–LUMO gaps [eV] of corroles P(tpfc)(OH)₂, **1-P**, **2-P**, **3-P** and **4-P**.

MO	P(tpfc)(OH) ₂	1-P	2-P	3-P	4-P
LUMO+1	-2.46	-2.62	-2.37	-2.32	-2.25
LUMO	-2.88	-2.99	-2.96	-2.92	-2.92
HOMO	-5.80	-5.89	-5.77	-5.70	-5.68
HOMO-1	-5.96	-5.93	-5.87	-5.80	-5.81
HLG ^[a]	2.92	2.91	2.81	2.79	2.76
OG ^[b]	2.33	2.29	2.27	2.25	2.25
FG ^[c]	2.62	2.66	2.52	2.50	2.48

[a] HOMO–LUMO gap calculated from the energy gap between the computed HOMO and LUMO. [b] Optical gap corresponding to the energy of the first electronic transition. [c] Fundamental gap representing the difference between the ionization potential and the electron affinity (see computational details in the Experimental Section).^[23]

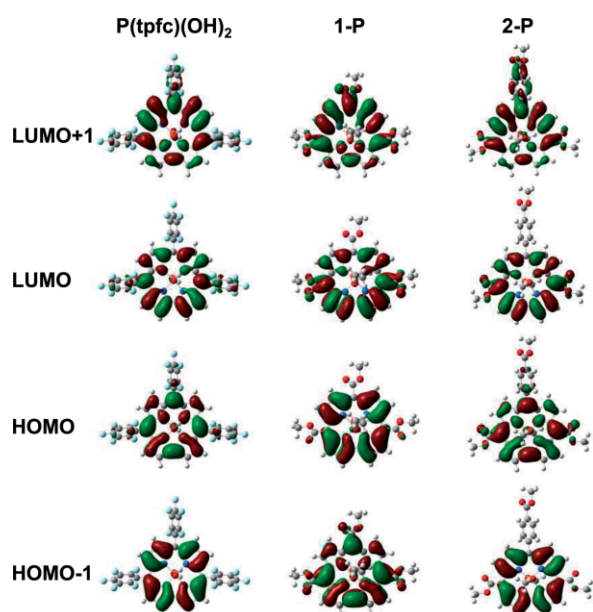


Figure 5. Plots of the frontier orbitals of P(tpfc)(OH)₂, **1-P** and **2-P**.

According to the Gouterman model, the absorption bands arise from transitions between the two highest occupied

Table 4. Compositions, vertical excitation energies [nm] and oscillator strengths (*f*) of the lowest optically allowed electronic transitions of corroles **1-P** and **2-P**.

	<i>E</i> [nm]	<i>f</i>	Composition [%]
1-P	542	0.057	HOMO→LUMO (66), HOMO-1→LUMO+1 (18), HOMO-1→LUMO (10)
1-P	539	0.051	HOMO-1→LUMO (18), HOMO-1→LUMO+1 (20), HOMO→LUMO (52), HOMO→LUMO+1 (10)
1-P	407	1.088	HOMO-1→LUMO (34), HOMO→LUMO+1 (65)
1-P	405	0.855	HOMO-1→LUMO+1 (71), HOMO→LUMO (27)
2-P	545	0.183	HOMO-1→LUMO+1 (20), HOMO→LUMO (79)
2-P	535	0.069	HOMO-1→LUMO (75), HOMO→LUMO+1 (24)
2-P	403	1.060	HOMO-1→LUMO (23), HOMO→LUMO+1 (74)
2-P	391	0.991	HOMO-1→LUMO+1 (78), HOMO→LUMO (20)

(HOMO-1 and HOMO) and two lowest unoccupied (LUMO and LUMO+1) orbitals. These two sets of orbitals are almost degenerate, and both are composed of a symmetric and a nonsymmetric orbital with respect to the plane orthogonal to the macrocycle and comprising the P and C10 atoms. We note that no electron density appears at the phosphorus centre (with very slight contributions from the two hydroxido ligands). In contrast, one can observe electron density at all *meso* positions for the symmetric orbitals [LUMO+1 and HOMO (HOMO-1 for **1-P**)], whereas the asymmetric ones [LUMO and HOMO-1 (HOMO for **1-P**)] present density only at the *meso* carbon atoms C5 and C15. In most of the orbitals, these latter atoms also share electron density with their connected ester groups. This π overlap explains the electron-withdrawing character displayed by the 5,15-*meso*-ester groups.

The replacement of the three pentafluorophenyl groups of P(tpfc)(OH)₂ by ester ones in **1-P** produces a strong stabilization of the LUMOs and of the HOMO orbitals, whereas the HOMO-1 is destabilized, which leads to an inversion in the energies of the two frontier occupied orbitals. If the electron-withdrawing strength of the 10-*meso* substituent is decreased, the LUMO is slightly stabilized, whereas the other three orbitals are destabilized. The *meso*-ester groups are consequently interesting stabilizing groups; however, as they impact all of the orbitals almost equally, the HOMO–LUMO electrochemical gap (Table 2) as well as the absorption and emission properties are barely modified if the pentafluorophenyl groups are replaced by ester ones, which are also less sterically hindered.

Conclusions

As in the free-base series, ester substituents at the 5- and 15-positions of phosphorus(V) *meso*-substituted corroles have a strong electron-withdrawing character, which even exceeds that of pentafluorophenyl groups. This efficiency probably results from the low steric hindrance of ester moieties, which allows a good π overlap with the aromatic system of the macro-

cycle. Nevertheless, as these groups stabilized both the HOMOs and LUMOs of the complexes, they only slightly tune the light absorption and emission properties with respect to those of the corresponding *meso*-triaryl derivatives. These conclusions were extracted from an extensive study of the physicochemical properties of four hexacoordinate phosphorus(V) 5,15-ester corroles differing by the nature of the third *meso* substituent, which, unexpectedly, has a significant impact on the amplitude of the ruffling of the macrocycle. Indeed, this out-of-plane distortion increases with the electron deficiency of the peripheral substituent. Although the underlying relationship remains to be clarified, the trend observed in the present work is in accordance with a previous report.^[20] One of the issues accompanying the use of corrole derivatives is their stability towards oxidative conditions, which is usually enhanced by electron-withdrawing *meso*-aryl groups. The present work shows that less sterically hindered ester groups are a valuable alternative to stabilize this class of compounds while maintaining their useful features, such as fluorescence or macrocycle distortion.

Experimental Section

Materials: All reagents were used as received. Dichloromethane and *n*-heptane were distilled over calcium hydride. Flash column chromatography was performed with silica gel 60 (230–400 mesh).

Physical Measurements: ¹H NMR spectra were recorded with a Bruker Avance 400 Ultrashield NMR spectrometer. The ¹H NMR chemical shifts are given in ppm and were referenced to the residual peaks of CDCl₃ (δ = 7.26 ppm) or CD₃OD (δ = 3.31 ppm). The UV/Vis absorption spectra were recorded with a Shimadzu UV-2401 (PC) instrument or with a Varian Cary 50 instrument. The emission spectra were recorded with a Horiba–Jobin Yvon Fluorolog-3 spectrofluorimeter equipped with a three-slit double-grating excitation and a spectrograph emission monochromator with dispersions of 2.1 nm/mm (1200 grooves per mm). The steady-state luminescence was excited by unpolarized light from a 450 W xenon continuous wave (CW) lamp and detected at an angle of 90° for dilute solution measurements (10 mm quartz cell) with a red-sensitive Hamamatsu R928 photomultiplier tube. The luminescence quantum yields (Φ_f) were measured in dilute dichloromethane or toluene solutions with an absorbance below 0.1 and calculated with [Equation (1)], in which OD(λ) is the absorbance at the excitation wavelength (λ), *n* is the refractive index, and *I* is the integrated luminescence intensity. The subscripts “r” and “x” stand for reference and sample, respectively.

$$\Phi_{f,x}/\Phi_{f,r} = [\text{OD}(\lambda)/\text{OD}_x(\lambda)][I_x/I_r] [n_x^2/n_r^2] \quad (1)$$

The luminescence quantum yields were not corrected for the refractive indices. 5,10,15,20-Tetraphenylporphyrin (TPP) in aerated toluene was used as a standard with $\Phi_{f,r} = 0.11$.^[21]

For the time-resolved fluorescence emission, the measurements were performed with a Horiba–Jobin Yvon IBH Fluorolog-3 spectrofluorimeter that was adapted for time-correlated single-photon counting. For these measurements, pulsed light-emitting diodes (LEDs) with an appropriate wavelength were used ($\lambda_{\text{ex}} = 540$ nm). The emission was monitored perpendicular to the excitation pulse, and spectroscopic selection was achieved by passage through the spectrograph. A thermoelectrically cooled single-photon-detection module (Horiba–Jobin Yvon IBH, TBX-04-D) that incorporated a fast-

rise-time photomultiplier tube, a wide-bandwidth preamplifier and a picosecond-constant fraction discriminator was used as the detector. The signals were acquired with an IBH DataStation Hub photon-counting module, and data analysis was performed with the commercially available DAS 6 decay-analysis software package from Horiba–Jobin Yvon IBH; the reported τ values are given with an estimated uncertainty of ca. 10 %.

The HRMS-ESI and MS analyses were performed with a QStar Elite (Applied Biosystems SCIEX) spectrometer or a SYNAPT G2 HDMS (Waters) spectrometer. These two instruments were equipped with electrospray ionization sources and were used in the positive-ion mode with the capillary voltage set at +5500 V.

The cyclic voltammetric data were acquired with a BAS 100 potentiostat (Bioanalytical Systems) and a PC with the BAS100W software (v2.3). A three-electrode system with a Pt working electrode (diameter 1.6 mm), a Pt counter electrode and a Ag/AgCl (with 3M NaCl filling solution) reference electrode were used. [*n*Bu₄N][PF₆] (0.1 M in CH₂Cl₂) served as an inert electrolyte. The cyclic voltammograms were recorded at a scan rate of 100 mV/s. Ferrocene was used as an internal standard.^[25]

Crystal-Structure Determination: The intensity data for **1-P** and **3-P** were collected with a Bruker–Nonius Kappa CCD diffractometer with Mo-*K*_α radiation ($\lambda = 0.71073$ Å). The data collection was performed with COLLECT,^[26] and cell refinement and data reduction were performed with DENZO/SCALEPACK.^[27] The intensity data for **2-P** and **4-P** were collected with a Rigaku Oxford Diffraction Supernova diffractometer with Cu-*K*_α radiation ($\lambda = 1.54184$ Å). The data collection, cell refinement and data reduction were performed with CrysAlisPro (Rigaku Oxford Diffraction). The crystal for **2-P** appeared to be a twin, and only the major domain was indexed and used for structure resolution. The structures were solved with SIR92^[28] or SHELXS,^[29] and SHELXL-2013^[29] was used for full-matrix least-squares refinements. The hydrogen atoms were introduced at geometrical positions and their *U*_{iso} parameters were fixed to 1.2*U*_{eq} (parent atom) for the aromatic or CH₂ carbon atoms and to 1.5*U*_{eq} (parent atom) for the methyl groups.

CCDC 1471252 (for **3-P**), 1471253 (for **1-P**), 1471254 (for **2-P**) and 1471255 (for **4-P**) contain the supplementary crystallographic data for this paper. These data can be obtained free of charge from The Cambridge Crystallographic Data Centre.

Computational Details: All TD-DFT and DFT calculations were performed with the Gaussian 09 D01 program.^[30] We use tightened self-consistent field (at least 10⁻¹⁰ a.u.) and geometry optimization (10⁻⁵ a.u.) convergence thresholds, and an improved DFT integration grid (the so-called ultrafine grid, a pruned 99,590 grid). The macrocycles were modelled by replacing the C₁₆H₃₃ alkyl chains and Et groups with Me groups to save computational time. These calculations relied on the PBE0 hybrid functional.^[31] Following a basis set combination approach,^[32] we used the 6-31G(d) atomic basis set to determine the geometrical and vibrational parameters, whereas the transition energies and the gaps (*G*, see below) were computed with 6-311+G(2d,p). The nature of all stationary points was confirmed by analytical Hessian calculations that returned zero imaginary vibrational modes (minima). Environmental effects (here, dichloromethane) were accounted for by the linear-response (LR) polarizable continuum model (PCM),^[33] as implemented in Gaussian09.^[30] Non-equilibrium effects were taken into account for the absorption wavelengths. To allow a consistent comparison between the calculated and experimental spectra (see Figure S4), the latter measured in the wavelength scale were transformed in line shapes by previously reported procedures.^[34] Several definitions of gap can

be given;^[23] therefore, here they were computed as: (1) the energetic difference between the HOMO and LUMO (HLG), (2) the energy corresponding to the first transition (OG) and (3) the differences between the ionization potential (IP) and the electron affinity (EA) determined according to the Koopmans theorem (FG). For the latter, we underline that we computed the energy of the cationic and anionic species with the optimized geometry of the neutral species.

Synthetic Methods: The corrole free bases were prepared as reported previously.^[10]

Compound 1-P: To a solution of 5,10,15-tris(ethoxycarbonyl)corrole (30 mg, 0.06 mmol) in dry pyridine (5 mL) was added POCl₃ (0.56 mL, 6 mmol), and the reaction mixture was heated to reflux for 30 min under argon. The solution color changed immediately from deep green to purple-violet with a greenish tint. The progress of the reaction was monitored by TLC analysis, and its completion was determined by absorption spectroscopy. After the completion of the reaction, the solvent was evaporated under reduced pressure. The crude solid was purified by silica gel chromatography (CH₂Cl₂/CH₃OH 50:1), and the desired compound was collected from a greenish pink-violet band. The solvent was evaporated to afford a deep purple-violet solid. Compound 1-P was crystallized from CH₂Cl₂/*n*-heptane to afford a purple solid (69%, 25 mg, 0.041 mmol). Single crystals of 1-P were grown by the slow diffusion of *n*-heptane into a concentrated solution of 1-P in dichloromethane containing few drops of methanol. *R*_f = 0.26 (silica, CH₂Cl₂/CH₃OH 20:1). ¹H NMR (400 MHz, CD₃OD, 25 °C): δ = 10.01 (dd, ³J_{H,H} = 5.1, ⁴J_{P,H} = 3.5 Hz, 2 H, β-H), 9.76 (dd, ³J_{H,H} = 4.7, ⁴J_{P,H} = 3.3 Hz, 2 H, β-H), 9.63 (dd, ³J_{H,H} = 5.2, ⁴J_{P,H} = 2.8 Hz, 2 H, β-H), 9.53 (dd, ³J_{H,H} = 4.7, ⁴J_{P,H} = 2.4 Hz, 2 H, β-H), 5.06 (m, 6 H, CO₂CH₂CH₃), 1.84 (t, ³J_{H,H} = 7.1 Hz, 6 H, CO₂CH₂CH₃), 1.80 (t, ³J_{H,H} = 7.2 Hz, CO₂CH₂CH₃) ppm. ³¹P NMR (160 MHz, CD₃OD, 25 °C): δ = -184.20 ppm. UV/Vis (CH₂Cl₂): λ_{max} (ε × 10⁻³) = 399 (42.0), 418 (210.7), 507 (3.0), 545 (8.5), 585 (22.4) nm. HRMS-ESI: calcd. for C₃₀H₂₉N₄O₈PNa [M + Na]⁺ 627.1620; found 627.1616.

Compound 2-P: To a solution of 10-(4-methoxycarbonylphenyl)-5,15-bis(ethoxycarbonyl)corrole (56 mg, 0.1 mmol) in dry pyridine (5 mL) was added POCl₃ (0.94 mL, 10 mmol), and the reaction mixture was heated to reflux for 30 min under argon. The solution color changed immediately from deep green to purple-violet with a greenish tint. The progress of the reaction was monitored by TLC analysis, and its completion was determined by absorption spectroscopy. After the completion of the reaction, the solvent was evaporated under reduced pressure. The crude solid was purified by silica gel chromatography (CH₂Cl₂/CH₃OH 50:1), and the desired compound was collected from a greenish pink-violet band. The solvent was evaporated to afford a deep purple-violet solid. Compound 2-P was crystallized from CH₂Cl₂/*n*-heptane to afford a purple solid (38%, 25 mg, 0.037 mmol). *R*_f = 0.48 (silica, CH₂Cl₂/CH₃OH 10:1). ¹H NMR (400 MHz, CD₃OD, 25 °C): δ = 9.97 (dd, ³J_{H,H} = 5.0, ⁴J_{P,H} = 3.6 Hz, 2 H, β-H), 9.81 (dd, ³J_{H,H} = 4.7, ⁴J_{P,H} = 3.6 Hz, 2 H, β-H), 9.55 (dd, ³J_{H,H} = 4.7, ⁴J_{P,H} = 2.3 Hz, 2 H, β-H), 8.90 (dd, ³J_{H,H} = 8.5, ⁴J_{P,H} = 5.7 Hz, 2 H, β-H), 8.50 (d, ³J_{H,H} = 8.4 Hz, 2 H, Ar-H), 8.34 (br s, 2 H, Ar-H), 5.04 (q, ³J_{H,H} = 7.2 Hz, 4 H, CO₂CH₂CH₃), 4.11 (s, 3 H, CO₂CH₃), 1.83 (t, ³J_{H,H} = 7.2 Hz, 6 H, CO₂CH₂CH₃) ppm. ³¹P NMR (160 MHz, CD₃OD, 25 °C): δ = -184.67 ppm. UV/Vis (CH₂Cl₂): λ_{max} (ε × 10⁻³) = 399 (61.1), 418 (228.4), 509 (3.9), 548 (9.8), 592 (37.8) nm. HRMS-ESI: calcd. for C₃₄H₂₈N₄O₇P [M - OCH₃]⁺ 635.1690; found 635.1691.

Compound 3-P: To a solution 10-(3,5-di-*tert*-butylphenyl)-5,15-bis(ethoxycarbonyl)corrole (63 mg, 0.1 mmol) in dry pyridine (5 mL) was added POCl₃ (0.94 mL, 10 mmol), and the reaction mixture was

heated to reflux for 30 min under argon. The solution color changed immediately from deep green to purple-violet with a greenish tint. The progress of reaction was monitored by TLC analysis, and its completion was determined by absorption spectroscopy. After the completion of the reaction, the solvent was evaporated under reduced pressure. The crude solid was purified by chromatography (CH₂Cl₂/CH₃OH 100:1) with basic alumina, and the desired compound was collected from a greenish pink-violet band. The solvent was evaporated to afford a deep purple-violet solid. Compound 3-P was crystallized from CH₂Cl₂/*n*-heptane to afford a purple solid (46% yield, 33 mg, 0.046 mmol). Single crystals of 3-P were grown serendipitously from a solution of 3-P in CD₃OD in an NMR tube. *R*_f = 0.35 (neutral alumina, CH₂Cl₂). ¹H NMR (400 MHz, CD₃OD, 25 °C): δ = 9.95 (dd, ³J_{H,H} = 5.0, ⁴J_{P,H} = 3.6 Hz, 2 H, β-H), 9.79 (dd, ³J_{H,H} = 4.7, ⁴J_{P,H} = 3.4 Hz, 2 H, β-H), 9.10 (dd, ³J_{H,H} = 4.6, ⁴J_{P,H} = 2.3 Hz, 2 H, β-H), 8.71 (dd, ³J_{H,H} = 5.0, ⁴J_{P,H} = 2.7 Hz, 2 H, β-H), 8.11 (br s, 1 H, Ar-H), 8.05 (br s, 1 H, Ar-H), 7.94 (t, ⁴J_{H,H} = 1.8 Hz, 1 H, Ar-H), 5.04 (q, ³J_{H,H} = 7.1 Hz, 4 H, CO₂CH₂CH₃), 1.83 (t, ³J_{H,H} = 7.1 Hz, 6 H, CO₂CH₂CH₃), 1.56 [d, ⁴J_{H,H} = 2.8 Hz, 18 H, C(CH₃)₃] ppm. ³¹P NMR (160 MHz, CD₃OD, 25 °C): δ = -184.80 ppm. UV/Vis (CH₂Cl₂): λ_{max} (ε × 10⁻³) = 399 (60.4), 418 (217.2), 510 (2.0), 550 (8.3), 594 (40.1) nm. HRMS-ESI: calcd. for C₄₀H₄₂N₄O₄P [M - OCH₃]⁺ 689.2887; found 689.2887.

Compound 4-P: To a solution of 10-octadecyl-5,15-bis(ethoxycarbonyl)corrole (13 mg, 0.02 mmol) in dry pyridine (5 mL) was added POCl₃ (0.19 mL, 2 mmol), and the reaction mixture was heated to reflux for 30 min under argon. The solution color changed immediately from deep green to purple-violet with a greenish tint. The progress of the reaction was monitored by TLC analysis, and its completion was determined by absorption spectroscopy. After the completion of the reaction, the solvent was evaporated under reduced pressure. The crude solid was purified by silica gel chromatography (CH₂Cl₂/CH₃OH 50:1), and the desired compound was collected from a greenish pink-violet band. The solvent was evaporated to afford a deep purple-violet solid (66%, 10 mg, 0.013 mmol). *R*_f = 0.75 (silica, CH₂Cl₂/CH₃OH 10:1). ¹H NMR (400 MHz, CD₃OD, 25 °C): δ = 10.01 (dd, ³J_{H,H} = 5.2, ⁴J_{P,H} = 3.7 Hz, 2 H, β-H), 9.74 (dd, ³J_{H,H} = 4.6, ⁴J_{P,H} = 3.3 Hz, 2 H, β-H), 9.61 (dd, ³J_{H,H} = 5.1, ⁴J_{P,H} = 2.9 Hz, 2 H, β-H), 9.46 (dd, ³J_{H,H} = 4.7, ⁴J_{P,H} = 2.3 Hz, 2 H, β-H), 5.03 (q, ³J_{H,H} = 7.1 Hz, 4 H, CO₂CH₂CH₃), 1.84 (t, ³J_{H,H} = 7.2 Hz, 6 H, CO₂CH₂CH₃), 1.29 (br s, 33 H, C₁₆H₃₃) ppm. ³¹P NMR (160 MHz, CD₃OD, 25 °C): δ = -185.20 ppm. UV/Vis (CH₂Cl₂): λ_{max} (ε × 10⁻³) = 401 (58.0), 418 (215.4), 511 (3.2), 552 (8.5), 598 (39.8) nm. HRMS-ESI: calcd. for C₄₂H₅₄N₄O₅P [M - OCH₃]⁺ 725.3826; found 725.3826.

Compound 5-P: To a solution of 3-P (15 mg, 0.02 mmol) in dry tetrahydrofuran (THF, 10 mL) was added NaBH₄ (7.6 mg, 0.2 mmol), and the reaction mixture was heated to reflux for 1 h under argon. The progress of the reaction was monitored by TLC analysis, and its completion was determined by absorption spectroscopy. After the completion of the reaction, the reaction was quenched with a H₂O/MeOH mixture. The mixture was extracted with CHCl₃. The organic layer was washed with brine and dried with anhydrous Na₂SO₄, and the solvents were evaporated to dryness. The crude solid was purified by silica gel chromatography (CH₂Cl₂/EtOAc 20:1). Compound 5-P was crystallized from CH₂Cl₂/*n*-heptane to afford a purple solid (30%, 4 mg, 6 μmol). *R*_f = 0.38 (silica gel, CH₂Cl₂). ¹H NMR (400 MHz, CDCl₃, 25 °C): δ = 9.99 (dd, ³J_{H,H} = 5.0, ⁴J_{P,H} = 1.6 Hz, 2 H, β-H), 9.84 (dd, ³J_{H,H} = 4.6, ⁴J_{P,H} = 2.0 Hz, 2 H, β-H), 9.43 (dd, ³J_{H,H} = 4.5, ⁴J_{P,H} = 1.0 Hz, 2 H, β-H), 9.02 (dd, ³J_{H,H} = 4.9, ⁴J_{P,H} = 1.4 Hz, 2 H, β-H), 8.19 (br s, 1 H, Ar-H), 7.93 (br s, 1 H, Ar-H), 7.83 (br s, 1 H, Ar-H), 5.04 (q, ³J_{H,H} = 7.1 Hz, 4 H, CO₂CH₂CH₃), 1.85 (t, ³J_{H,H} = 7.1 Hz, 6 H, CO₂CH₂CH₃), 1.57 [s, 9 H, C(CH₃)₃], 1.52 [s, 9 H, C(CH₃)₃], -2.40 (s, 2

H, PH) ppm. ^{31}P NMR (160 MHz, CDCl_3 , 25 °C): $\delta = -223.3$ ppm (d, $J_{\text{PH}} = 1100$ Hz, 1 H, PH). UV/Vis (CH_2Cl_2): λ_{max} ($\epsilon \times 10^{-3}$) = 429 (26.1), 443 (23.8), 600 (2.9), 635 (6.9) nm. MS-ESI: $m/z = 659.3$ [M - H] $^+$.

Acknowledgments

D. G. gratefully thanks the China Scholarship Council for granting his PhD fellowship in Marseille. C. A. acknowledges the Agence Nationale de la Recherche (ANR EMA) for her PhD grant. D. J. thanks the ANR and European Research Council (ERC) for financial support in the framework of the EMA and Marches-78845 grants, respectively. Calculations were performed using the resources of the GENCI-CINES/IDRIS, those of the Centre de Calcul Intensif des Pays de Loire as well as those of the local Troy cluster acquired thanks to Région des Pays de la Loire.

- [1] a) R. Guilard, D. T. Gryko, G. Canard, J.-M. Barbe, B. Koszarna, S. Brandès, M. Tasiar, *Org. Lett.* **2002**, *4*, 4491–4494; b) S. Nardis, D. Monti, R. Paolesse, *Mini-Rev. Org. Chem.* **2005**, *2*, 355–374; c) B. Koszarna, D. T. Gryko, *J. Org. Chem.* **2006**, *71*, 3707–3717; d) M. König, F. Faschinger, L. M. Reith, W. Schöffberger, *J. Porphyrins Phthalocyanines* **2016**, *20*, 96–107.
- [2] a) J. P. Collman, M. Kaplun, R. A. Decréau, *Dalton Trans.* **2006**, 554–559; b) I. Aviv, Z. Gross, *Chem. Commun.* **2007**, 1987–1999; c) I. Aviv-Harel, Z. Gross, *Chem. Eur. J.* **2009**, *15*, 8382–8394; d) R. Brimblecombe, G. C. Dismukes, G. F. Swiegers, L. Spiccia, *Dalton Trans.* **2009**, 9374–9384; e) A. N. Biswas, P. Das, A. Agarwala, D. Bandyopadhyay, P. Bandyopadhyay, *J. Mol. Catal. A* **2010**, *326*, 94–98.
- [3] a) C. Di Natale, C. Goletti, R. Paolesse, M. Drago, A. Macagnano, A. Mantini, V. I. Troitsky, T. S. Berzina, M. Cocco, A. D'Amico, *Sens. Actuators B* **1999**, *57*, 183–187; b) J.-M. Barbe, G. Canard, S. Brandès, R. Guilard, *Chem. Eur. J.* **2007**, *13*, 2118–2129; c) C. I. M. Santos, E. Oliveira, J. Fernández-Lodeiro, J. F. B. Barata, S. M. Santos, M. A. F. Faustino, J. A. S. Cavaleiro, M. G. P. M. S. Neves, C. Lodeiro, *Inorg. Chem.* **2013**, *52*, 8564–8572; d) C. I. M. Santos, *ChemistryOpen* **2014**, *3*, 88–92; e) R. Capuano, G. Pomarico, R. Paolesse, C. Di Natale, *Sensors* **2015**, *15*, 8121–8130.
- [4] a) D. Walker, S. Chappel, A. Mahammed, B. S. Brunschwig, J. R. Winkler, H. B. Gray, A. Zaban, Z. Gross, *J. Porphyrins Phthalocyanines* **2006**, *10*, 1259–1262; b) S.-L. Lai, L. Wang, C. Yang, M.-Y. Chan, X. Guan, C.-C. Kwok, C.-M. Che, *Adv. Funct. Mater.* **2014**, *24*, 4655–4665; c) D. Gao, J. Andeme Edzang, A. K. Diallo, T. Dutronc, T. S. Balaban, C. Videlot-Ackermann, E. Terazzi, G. Canard, *New J. Chem.* **2015**, *39*, 7140–7146.
- [5] a) A. Kanamori, M.-M. Catrinescu, A. Mahammed, Z. Gross, L. A. Levin, *J. Neurochem.* **2010**, *114*, 488–498; b) P. Lim, A. Mahammed, Z. Okun, I. Saltsman, Z. Gross, H. B. Gray, J. Termini, *Chem. Res. Toxicol.* **2012**, *25*, 400–409; c) D. Samaroo, E. Perez, A. Aggarwal, A. Wills, N. O'Connor, *Ther. Delivery* **2014**, *5*, 859–872.
- [6] a) S. Berg, K. E. Thomas, C. M. Beavers, A. Ghosh, *Inorg. Chem.* **2012**, *51*, 9911–9916; b) K. E. Thomas, C. M. Beavers, A. Ghosh, *Mol. Phys.* **2012**, *110*, 2439–2444; c) D. Gao, G. Canard, M. Giorgi, T. S. Balaban, *Eur. J. Inorg. Chem.* **2012**, 5915–5920.
- [7] a) R. Paolesse, S. Licoccia, G. Bandoli, A. Dolmella, T. Boschi, *Inorg. Chem.* **1994**, *33*, 1171–1176; b) D. Gao, G. Canard, M. Giorgi, P. Vanlout, T. S. Balaban, *Eur. J. Inorg. Chem.* **2014**, 279–287; c) J. Capar, J. Zonneveld, S. Berg, J. Isaksson, K. J. Gagnon, K. E. Thomas, A. Ghosh, *J. Inorg. Biochem.* **2016**, *162*, 146–153.
- [8] a) S. Hiroto, K. Furukawa, H. Shinokubo, A. Osuka, *J. Am. Chem. Soc.* **2006**, *128*, 12380–12381; b) L. S. H. P. Vale, J. F. B. Barata, M. G. P. M. S. Neves, M. A. F. Faustino, A. C. Tomé, A. M. S. Silva, F. A. A. Paz, J. A. S. Cavaleiro, *Tetrahedron Lett.* **2007**, *48*, 8904–8908; c) G. Pomarico, S. Nardis, M. Stefanelli, D. O. Cicero, M. G. H. Vicente, Y. Fang, P. Chen, K. M. Kadish, R. Paolesse, *Inorg. Chem.* **2013**, *52*, 8834–8844; d) M. Stefanelli, M. L. Naitana, M. Chiarini, S. Nardis, A. Ricci, F. R. Fronczek, C. Lo Sterzo, K. M. Smith, R. Paolesse, *Eur. J. Org. Chem.* **2015**, 6811–6816; e) B. Berionni Berna, S. Nardis, F. Mandoj, F. R. Fronczek, K. M. Smith, R. Paolesse, *Org. Biomol. Chem.* **2016**, *14*, 2891–2897; f) B. Berionni Berna, S. Nardis, P. Galloni, A. Savoldelli, M. Stefanelli, F. R. Fronczek, K. M. Smith, R. Paolesse, *Org. Lett.* **2016**, *18*, 3318–3321; g) S. Ooi, T. Tanaka, K. H. Park, D. Kim, A. Osuka, *Angew. Chem. Int. Ed.* **2016**, *55*, 6535–6539; *Angew. Chem.* **2016**, *128*, 6645–6649.
- [9] a) A. Mahammed, I. Goldberg, Z. Gross, *Org. Lett.* **2001**, *3*, 3443–3446; b) R. Paolesse, S. Nardis, M. Venanzi, M. Mastroianni, M. Russo, F. R. Fronczek, M. G. H. Vicente, *Chem. Eur. J.* **2003**, *9*, 1192–1197; c) M. Stefanelli, M. Mastroianni, S. Nardis, S. Licoccia, F. R. Fronczek, K. M. Smith, W. Zhu, Z. Ou, K. M. Kadish, R. Paolesse, *Inorg. Chem.* **2007**, *46*, 10791–10799; d) K. Sudhakar, V. Velkannan, L. Giribabu, *Tetrahedron Lett.* **2012**, *53*, 991–993; e) J. F. B. Barata, C. I. M. Santos, M. G. P. M. S. Neves, M. A. F. Faustino, J. A. S. Cavaleiro, *Top. Heterocycl. Chem.* **2014**, *33*, 79–141.
- [10] G. Canard, D. Gao, A. D'Aléo, M. Giorgi, F.-X. Dang, T. S. Balaban, *Chem. Eur. J.* **2015**, *21*, 7760–7771.
- [11] a) A. Ghosh, M. Ravikanth, *Chem. Eur. J.* **2012**, *18*, 6386–6396; b) G. Pomarico, S. Nardis, M. L. Naitana, M. G. H. Vicente, K. M. Kadish, P. Chen, L. Prodi, D. Genovese, R. Paolesse, *Inorg. Chem.* **2013**, *52*, 4061–4070; c) S. S. K. Raavi, J. Yin, G. Grancini, C. Soci, V. R. Soma, G. Lanzani, L. Giribabu, *J. Phys. Chem. C* **2015**, *119*, 28691–28700.
- [12] a) M. Shi, J. Tian, C. Mkhize, G. Kubheka, J. Zhou, J. Mack, T. Nyokong, Z. Shen, *J. Porphyrins Phthalocyanines* **2014**, *18*, 698–707; b) T. Furuyama, Y. Sugiya, N. Kobayashi, *Chem. Commun.* **2014**, *50*, 4312–4314; c) A. Preuß, I. Saltsman, A. Mahammed, M. Pfitzner, I. Goldberg, Z. Gross, B. Röder, *J. Photochem. Photobiol. B* **2014**, *133*, 39–46; d) C. Mkhize, J. Britton, J. Mack, T. Nyokong, *J. Porphyrins Phthalocyanines* **2015**, *19*, 192–204; e) A. Mahammed, Z. Gross, *Angew. Chem. Int. Ed.* **2015**, *54*, 12370–12373; *Angew. Chem.* **2015**, *127*, 12547–12550.
- [13] a) X. Liang, J. Mack, L.-M. Zheng, Z. Shen, N. Kobayashi, *Inorg. Chem.* **2014**, *53*, 2797–2802; b) Y.-G. Wang, Z. Zhang, H. Wang, H.-Y. Liu, *Bioorg. Chem.* **2016**, *67*, 57–63.
- [14] a) L. Giribabu, J. Kandhadi, R. K. Kanaparthi, *J. Fluoresc.* **2014**, *24*, 569–577; b) B. J. Brennan, Y. C. Lam, P. M. Kim, X. Zhang, G. W. Brudvig, *ACS Appl. Mater. Interfaces* **2015**, *7*, 16124–16130.
- [15] a) R. Paolesse, T. Boschi, S. Licoccia, R. G. Khoury, K. M. Smith, *Chem. Commun.* **1998**, 1119–1120; b) A. Ghosh, W.-Z. Lee, M. Ravikanth, *Eur. J. Inorg. Chem.* **2012**, 4231–4239; c) J. Vestfrid, R. Kothari, A. Kostenko, I. Goldberg, B. Tumanskii, Z. Gross, *Inorg. Chem.* **2016**, *55*, 6061–6067; d) T. Chatterjee, W.-Z. Lee, M. Ravikanth, *Dalton Trans.* **2016**, *45*, 7815–7822.
- [16] L. Simkhovich, A. Mahammed, I. Goldberg, Z. Gross, *Chem. Eur. J.* **2001**, *7*, 1041–1055.
- [17] K. M. Kadish, Z. Ou, V. A. Adamian, R. Guilard, C. P. Gros, C. Erben, S. Will, E. Vogel, *Inorg. Chem.* **2000**, *39*, 5675–5682.
- [18] a) F. Mandoj, S. Nardis, G. Pomarico, R. Paolesse, *J. Porphyrins Phthalocyanines* **2008**, *12*, 19–26; b) S. Nardis, G. Pomarico, F. Mandoj, F. R. Fronczek, K. M. Smith, R. Paolesse, *J. Porphyrins Phthalocyanines* **2010**, *14*, 752–757; c) L. Tortora, S. Nardis, F. R. Fronczek, K. M. Smith, R. Paolesse, *Chem. Commun.* **2011**, *47*, 4243–4245; d) M. Fasciotti, A. F. Gomes, F. C. Gozzo, B. A. Iglesias, G. F. de Sá, R. J. Daroda, M. Toganoh, H. Furuta, K. Araki, M. N. Eberlin, *Org. Biomol. Chem.* **2012**, *10*, 8396–8402.
- [19] a) C. Tardieux, C. P. Gros, R. Guilard, *J. Heterocycl. Chem.* **1998**, *35*, 965–970; b) R. Paolesse, F. Sagone, A. Macagnano, T. Boschi, L. Prodi, M. Montalti, N. Zaccaroni, F. Bolletta, K. M. Smith, *J. Porphyrins Phthalocyanines* **1999**, *3*, 364–370; c) M. O. Senge, N. N. Sergeeva, *Angew. Chem. Int. Ed.* **2006**, *45*, 7492–7495; *Angew. Chem.* **2006**, *118*, 7654–7657; d) P. Świder, A. Nowak-Król, R. Voloshchuk, J. P. Lewtak, D. T. Gryko, W. Danikiewicz, *J. Mass Spectrom.* **2010**, *45*, 1443–1451; e) J. Wojaczyński, M. Duszak, L. Latos-Grażyński, *Tetrahedron* **2013**, *69*, 10445–10449; f) J. Wojaczyński, *Top. Heterocycl. Chem.* **2014**, *33*, 143–202.
- [20] G. Pomarico, L. Tortora, F. R. Fronczek, K. M. Smith, R. Paolesse, *J. Inorg. Biochem.* **2016**, *158*, 17–23.
- [21] P. G. Seybold, M. Gouterman, *J. Mol. Spectrosc.* **1969**, *31*, 1–13.
- [22] P. L. Muiño, P. R. Callis, *J. Phys. Chem. B* **2009**, *113*, 2572–2577.
- [23] J.-L. Bredas, *Mater. Horiz.* **2014**, *1*, 17–19.
- [24] A. D. Laurent, D. Jacquemin, *Int. J. Quantum Chem.* **2013**, *113*, 2019–2039.
- [25] N. G. Connelly, W. E. Geiger, *Chem. Rev.* **1996**, *96*, 877–910.

- [26] *Nonius COLLECT*, Nonius BV, Delft, **2001**.
- [27] Z. Otwinowski, W. Minor in *Methods in Enzymology* (Eds.: C. W. Carter Jr., R. M. Sweet), Academic Press, New York, **1997**, pp. 307–326.
- [28] A. Altomare, G. Casciaro, G. Giacovazzo, A. Guagliardi, M. C. Burla, G. Polidori, M. Camalli, *J. Appl. Crystallogr.* **1994**, *27*, 435.
- [29] G. M. Sheldrick, *Acta Crystallogr., Sect. A* **2008**, *64*, 112.
- [30] M. J. Frisch, G. W. Trucks, H. B. Schlegel, G. E. Scuseria, M. A. Robb, J. R. Cheeseman, G. Scalmani, V. Barone, B. Mennucci, G. A. Petersson, H. Nakatsuji, M. Caricato, X. Li, H. P. Hratchian, A. F. Izmaylov, J. Bloino, G. Zheng, J. L. Sonnenberg, M. Hada, M. Ehara, K. Toyota, R. Fukuda, J. Hasegawa, M. Ishida, T. Nakajima, Y. Honda, O. Kitao, H. Nakai, T. Vreven, J. A. Montgomery Jr., J. E. Peralta, F. Ogliaro, M. Bearpark, J. J. Heyd, E. Brothers, K. N. Kudin, V. N. Staroverov, R. Kobayashi, J. Normand, K. Raghavachari, A. Rendell, J. C. Burant, S. S. Iyengar, J. Tomasi, M. Cossi, N. Rega, J. M. Millam, M. Klene, J. E. Knox, J. B. Cross, V. Bakken, C. Adamo, J. Jaramillo, R. Gomperts, R. E. Stratmann, O. Yazyev, A. J. Austin, R. Cammi, C. Pomelli, J. W. Ochterski, R. L. Martin, K. Morokuma, V. G. Zakrzewski, G. A. Voth, P. Salvador, J. J. Dannenberg, S. Dapprich, A. D. Daniels, Ö. Farkas, J. B. Foresman, J. V. Ortiz, J. Cioslowski, D. J. Fox, *Gaussian 09, Revision D.01*, Gaussian, Inc., Wallingford CT, **2009**.
- [31] C. Adamo, V. Barone, *J. Chem. Phys.* **1999**, *110*, 6158–6170.
- [32] B. Le Guennic, D. Jacquemin, *Acc. Chem. Res.* **2015**, *48*, 530–537 and references therein.
- [33] J. Tomasi, B. Mennucci, R. Cammi, *Chem. Rev.* **2005**, *105*, 2999–3093.
- [34] F. J. Avila Ferrer, J. Cerezo, E. Stendardo, R. Improta, F. Santoro, *J. Chem. Theory Comput.* **2013**, *9*, 2072–2082.